EPITAXIALLY-ENCAPSULATED QUAD MASS GYROSCOPE WITH NONLINEARITY COMPENSATION

Parsa Taheri-Tehrani[1], Mitchell Kline[2], Igor Izyumin[2], Burak Eminoglu[2], Yu-Ching Yeh[2], Yushi Yang[3], Yunhan Chen[3], Ian Flader[3], Eldwin J. Ng[3], Thomas W. Kenny[3], Bernhard E. Boser[2], and David A. Horsley[1]

[1]University of California, Davis, USA

[2]University of California, Berkeley, USA

[3]Stanford University, Stanford, USA

ABSTRACT

We present an epitaxially-encapsulated 2x2 mm^2 quad-mass gyroscope (QMG). Relative to the earlier QMG which measured 8x8 mm^2 and required an external vacuum package and getter [1], this device is 16x smaller in area and is vacuum-sealed at the wafer-level. Due to the device's small size, high quality factor (Q) and large oscillation amplitude are required to achieve low noise. However, the device's high Q (85,000) makes it highly sensitive to mechanical nonlinearity, resulting in amplitude-frequency dependence and instability of the oscillator loop at large amplitudes. To overcome these problems, we demonstrate electrostatic compensation of the mechanical nonlinearity, enabling 10x greater amplitude and therefore scale factor (SF). Together with closed-loop amplitude control and quadrature compensation, this enables angle-random walk of 0.42 mdeg/s/√Hz, comparable to the best QMG published to date. Closed-loop amplitude control and quadrature null are used to achieve a bias instability of 1.6 deg/hr.

INTRODUCTION

The principle of the vibratory gyroscope is Coriolis acceleration coupling between two resonant modes of a vibratory structure. One mode is driven at its resonance and, when rotation rate is applied, the Coriolis force induced on the second mode provides a measure of this rotation rate. The measure of coupling between the two resonances is known as angular gain, which is solely dependent on the geometry and mode shape of the resonator. Gyroscopes can be operated in mode-matched condition [2] or mode mismatched condition [3]. While mode-matched gyroscopes have greater sensitivity, careful structural design and/or electrostatic tuning is needed to make mode-matching possible [4]. In all types of vibratory gyroscopes, the sensitivity is increased by having large amplitude in the driven vibration mode and having a high quality factor (Q) in the sensing mode [5-6].

High quality factor resonators are highly sensitive to nonlinearities occurring at large vibration amplitudes [7]. One such nonlinearity is a cubic stiffness term that produces Duffing oscillator behavior, where the peak of the frequency response shifts depending on the oscillation amplitude. This nonlinear stiffness can have both mechanical and electrical origin. Mechanical tensile stiffening of the flexures is known to produce a spring-hardening nonlinearity. Conversely, electrostatic nonlinearity created by parallel-plate electrodes is associated with a spring-softening nonlinearity.

In this paper, we present a quad mass gyroscope (QMG) [8], illustrated in Figure 1. The QMG has four masses, each with four frames having parallel-plate electrodes for electrostatic drive, capacitive sense, and frequency tuning. The average resonant frequency of 8 devices was measured to be 21237±300 Hz with an average frequency difference of 117±80 Hz between the two resonant modes. The resonant frequency of the QMG used in rate-sensing experiments in this paper is ~21.35 kHz with 80 Hz split between the two resonance modes. For each mode, two electrodes are used for driving, two electrodes for differential sensing and four electrodes for frequency tuning, resulting in a total of sixteen electrodes. Table 1 summarizes key parameters of the gyroscope.

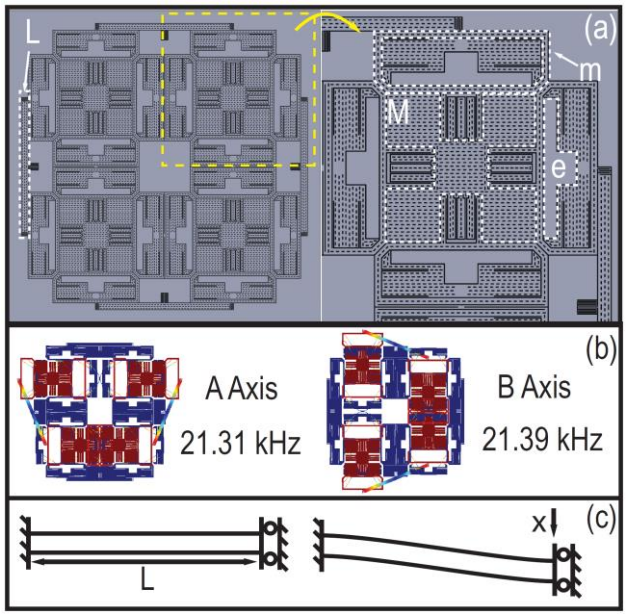

Fig. 1: (a) 2 mm device layout showing M: proof mass, m: drive frames, L: lever, and e: electrodes. (b) FEM-simulated mode shapes and natural frequencies of the two axes (c) Schematic of clamped-roller beams used in design.

Table 1: Gyroscope parameters

Parameter	Value	Units
Modal mass	123	µg
Modal stiffness	2300	N/m
Electrode area	0.017	mm^2
Electrode gap	1.5	µm
Angular gain	0.75	---
Quality factor	85,000	---
ARW	0.42	mdeg/s/√Hz
Bias Instability	1.6	deg/hr

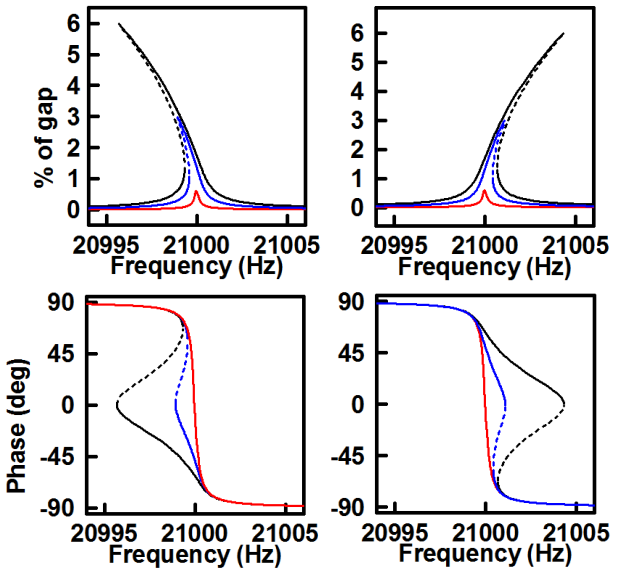

Fig. 2. Simulated frequency response plots of resonators exhibiting different nonlinearities at increasing amplitudes. The amplitude axes are normalized to the parallel-plate electrode gap. The figures on the left correspond to electrostatic nonlinearity, those on the right to mechanical nonlinearity.

RESONATOR DYNAMICS

The QMG's nonlinear behavior at resonance is described by the Duffing equation:

$$\ddot{u} + \frac{\omega_n}{Q}\dot{u} + \omega_n^2 u + \frac{k_3}{m}u^3 = F \qquad (1)$$

where u represents displacement, ω_n is the natural frequency, Q is the quality factor, m the modal mass, and k_3 is the stiffness coefficient corresponding to the cubic nonlinearity of the resonator. The sign of k_3 determines whether spring-softening (negative), or spring-hardening (positive) is present. Simulations of the Duffing oscillator's frequency response were conducted using parameters similar to those of the QMG and are shown in Figure 2. In these simulations, $k_3 = \pm 1178\times10^{11}$ (N/m^3), a value consistent with the QMG's parameters. The resonator's frequency response is linear up to an amplitude equal to 0.5% of the capacitive gap, whereas at a 6% amplitude, the response is significantly nonlinear. One means of quantifying this nonlinearity is the frequency shift of the resonant peak. At 6% amplitude, this is 4.5 Hz (0.02% when normalized to the 21 kHz linear resonant frequency and 1875% when normalized to the 240 mHz bandwidth of resonator).

The nonlinearities of the QMG were modeled and the results are summarized in Table 2. A model for the 3rd order mechanical nonlinearity in beams is discussed in [7]; however, the equations provided for cantilever beams should be modified to equation (2) to be applicable for the clamped-roller beams (Figure 1(c)) used in this QMG:

$$k_{3m} = \frac{0.5k_o}{b^2} \quad , \quad k_o = \frac{Ehb^3}{L^3} \qquad (2)$$

where E is the elastic modulus of silicon, k_o is the linear stiffness of the beam, b is the width, h the height, and L the length of the beam. Other types of springs such as folded springs and shuttle springs have negligible nonlinearities compared to clamped-clamped and clamped-roller beams. The electrostatic cubic nonlinearity can be calculated using the equation presented in [7]:

$$k_{3e} = -2\frac{\varepsilon_0 A}{g^5}V_b^2 \qquad (3)$$

where ε_o is vacuum permittivity, A and g are respectively the electrode area and electrode gap, and V_b is the voltage across the electrodes.

Referring to (2) and (3), the mechanical and electrostatic nonlinearities have opposite signs. The voltage dependence of the electrostatic nonlinearity makes it possible to adjust the value the electrostatic nonlinearity such that it cancels the mechanical nonlinearity. At one optimum voltage [9], the total cubic nonlinearity will be near zero and the gyroscope will show linear behavior. This voltage is calculated to be $\bar{V}_b = 34.3V$ from the parameters in Table 2. Experiments were conducted with the QMG resonator driven closed-loop using a PLL to control the resonator phase. This setup ensures that the oscillation frequency corresponds to the maximum point of the resonator's frequency response [10]. By varying the oscillation amplitude, this enabled measurement of the QMG's amplitude-frequency dependence at different bias voltages, shown in Figure 3. In an ideal linear resonator, changing the amplitude would have no effect on the oscillation frequency, and a straight vertical line would be

Table 2: Cubic nonlinearity calculations

type	Nominal Parameters	Estimated Parameters	k_3 (N/m^3)	#	Total cubic nonlinearity (N/m^3)
Mechanical Springs	L = 142 µm b = 3 µm h = 40 µm	L = 142 µm $\hat{b}$ = 2.9 µm h = 40 µm	3.363×10^{12}	32	1.076×10^{14}
	L = 241.5 µm b = 5.5 µm h = 40 µm	L = 241.5 µm $\hat{b}$ = 5.4 µm h = 40 µm	1.273×10^{12}	8	1.018×10^{13}
Parallel Plate Electrodes	A = 0.017 mm^2 g = 1.5 µm	A = 0.017 mm^2 $\hat{g}$ = 1.65 µm	$-2.509\times10^{10}V_b^2$	4	$1.003\times10^{11}V_b^2$
Total					$(1178\text{-}1.003V_b^2)\times10^{11}$

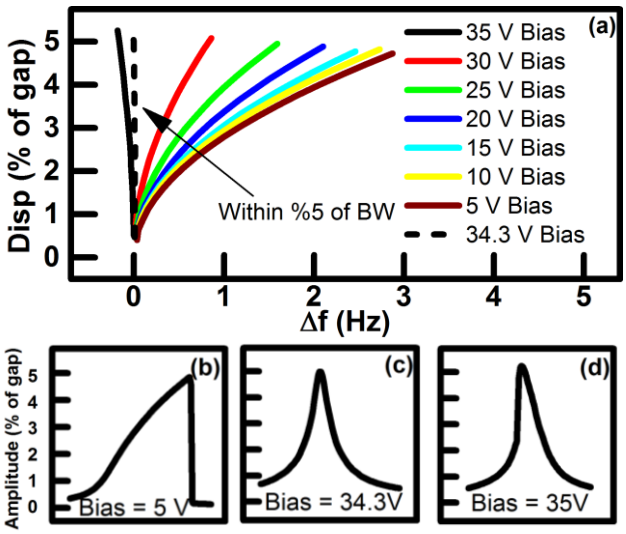

Fig. 3: (a) Amplitude-frequency dependence at various bias voltages. At $\overline{V}_b = 34.3V$, the behavior is linear. Frequency response when (b) $V_b < \overline{V}_b$, mechanical spring-stiffening dominates; (c) $V_b = \overline{V}_b$, nonlinearity is compensated at optimum bias, and (d) $V_b > \overline{V}_b$, electrostatic spring-softening dominates.

observed. At low bias voltage, spring-hardening is dominant and the amplitude-frequency slope is positive. At the optimum bias of $\overline{V}_b = 34.3V$ the minimum change in frequency is measured and the plot is nearly vertical. At voltages higher than $\overline{V}_b$, electrostatic spring-softening dominates and the slope is negative. At the optimum voltage, the frequency change is within 5 % of the BW.

GYROSCOPE PERFORMANCE

Electrostatic tuning was used to mode-match the QMG. Figure 4 illustrates the as-fabricated and mode-matched frequency response. Mode-matching increases Coriolis coupling and therefore scale-factor (SF) but also

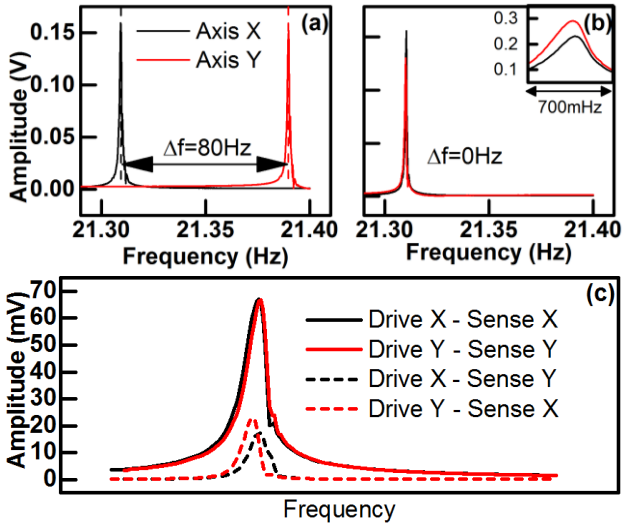

Fig. 4: Frequency sweep (a) as-fabricated (b) mode-matched. (c) When mode-matched, large coupling is observed between the axes when the quadrature nulling loop is inactive.

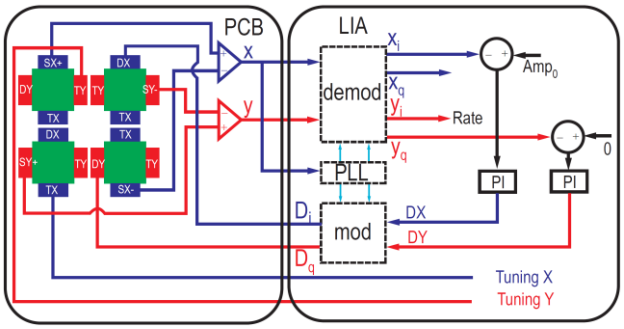

Fig. 5: Block diagram. Two PI controllers maintain in-phase drive amplitude (x_i) and null the sense-axis quadrature (y_q).

increases undesired coupling arising from imperfections in the structure. Due to the gyro's small mechanical bandwidth (0.24 Hz), it is very sensitive to amplitude and quadrature error fluctuations. To reduce these error sources, closed-loop amplitude control of the drive mode and a closed-loop quadrature nulling loop were used to minimize the fluctuations in amplitude of the drive mode and the quadrature in the sense mode, Figure 5. As a result of quadrature nulling, the fluctuation in the in-phase channel of the sense axis is also minimized. When operated closed-loop, the quadrature null controller reduces the initial quadrature from 2.6°/s to a level below the gyro's noise-floor. A Zurich Instruments lock-in-amplifier was used to implement the PLL and closed-loop controllers.

The scale-factor of the mode-matched gyroscope was measured both with and without the closed loop controllers. Sinusoidal rate inputs were applied using a rate-table oscillating with 5 degrees amplitude at frequencies from 0.1 Hz to 1 Hz. The measured frequency response is illustrated in Figure 6, showing a 240 mHz 3dB bandwidth, determined by the mechanical bandwidth of the QMG resonance, f_0/Q.

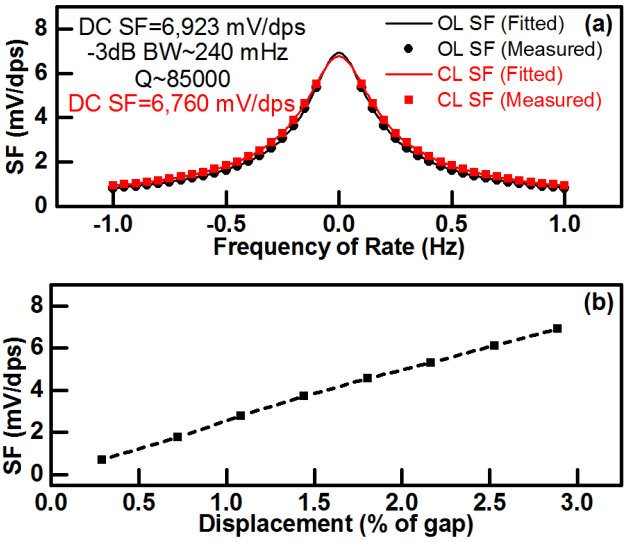

Fig. 6: Rate-table measurements. (a) Frequency response measured with swept-frequency rate input. OL: open-loop. CL: closed-loop amplitude control and quadrature null active. (b) The scale-factor (SF) increases linearly with drive-axis amplitude.

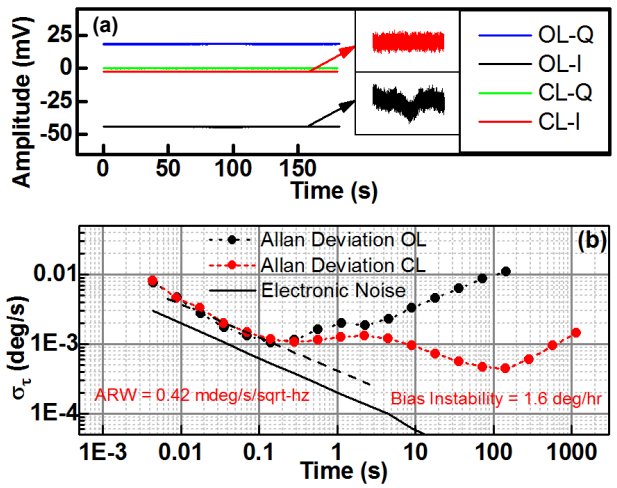

Fig. 7: (a) ZRO of open-loop and closed-loop operation (b) Allan deviation of open-loop and closed-loop operation. The amplitude control & quadrature null loops result in low bias instability (1.6 deg/hr). The ARW (0.42 mdeg/s/√Hz) is limited by Brownian noise.

To measure the noise floor of the gyroscope, the zero rate output (ZRO) was measured both with and without the closed-loop amplitude and quadrature controllers. Figure 7 shows the time-domain ZRO data and the Allan deviation analysis. As a result of the amplitude controller, the variation of the in-phase portion of the sense channel decreases. Adding the quadrature null loop on the sense channel further stabilizes the variation of the in-phase signal and also decreases the offset of this signal as shown in Figure 7(a). Allan deviation analysis in Figure 7(b) illustrates the improvement in the stability of the sense channel, resulting in a bias instability of 1.6 deg/hr. The measured ARW is 0.42 mdeg/s/√Hz and is dominated by Brownian noise which is over two times greater than the measured electronic noise floor.

CONCLUSION

In this paper we have presented a QMG operating at large displacement by nonlinearity compensation, resulting in 10x higher scale factor and subsequently lower ARW and bias instability. Voltage-dependent electrostatic nonlinearity was used to compensate for geometry-dependent mechanical nonlinearity, making it possible to operate the drive axis at large amplitude. The stability of the sense channel was further improved using a closed-loop amplitude controller on the drive axis and a closed-loop quadrature null controller on the sense channel.

ACKNOWLEDGEMENTS

This work was supported by DARPA under grant W31P4Q-11-1-0003. The authors would like to also thank Dr. Martial Defoort, post-doctoral scholar in the UC Davis MEMS Lab for discussions regarding nonlinearity.

REFERENCES

[1] A.A. Trusov, G. Atikyan, D.M. Rozelle, A.D. Meyer, S.A. Zotov, B.R. Simon, A.M. Shkel, "Flat Is Not Dead: Current and Future Performance of Si-MEMS Quad Mass Gyro (QMG) System," *IEEE/ION PLANS 2014*, Monterey, CA, USA, May 6-7, 2014.

[2] T.-H. Su, S. H. Nitzan, P. Taheri-Tehrani, M. H. Kline, B. E. Boser, D. A. Horsley, "Silicon MEMS Disk Resonator Gyroscope With an Integrated CMOS Analog Front-End," *IEEE Sensor journal,* vol.14, no.10, pp.3426-3432, Oct. 2014.

[3] S. Sonmezoglu, P. Taheri-Tehrani, C. Valzasina, L. Falorni, S. Zerbini, S. Nitzan, D. A. Horsley, "Single-Structure Micromachined 3-Axis Gyroscope with Reduced Drive-Force Coupling," *IEEE Electron Device Letters*, vol.36, no.9, pp.953-956, Sept. 2015.

[4] P. Taheri-Tehrani, T.-H. Su, A. Heidari, G. Jaramillo, C. Yang, S. Akhbari, H. Najar, S. Nitzan, D. Saito, L. Lin, D. A. Horsley, "MICRO-SCALE DIAMOND HEMISPHERICAL RESONATOR GYROSCOPE," *Solid-State Sensors, Actuators And Microsystems Workshop,* Hilton Head, South Carolina, June 2014.

[5] A. Heidari, M.-L. Chan, H.-A. Yang, G. Jaramillo, P. Taheri-Tehrani, P. Fonda, H. Najar, K. Yamazaki, L. Lin, D. A. Horsley, "Micromachined polycrystalline diamond hemispherical shell resonators," *Solid-State Sensors, Actuators and Microsystems (TRANSDUCERS & EUROSENSORS XXVII),* pp.2415-2418, 16-20 June 2013.

[6] P. Taheri-Tehrani, O. Izyumin, I. Izyumin, C. H. Ahn, E. J. Ng, V. Hong, Y. Yang, T. W. Kenny, B. E. Boser, D. A. Horsley, "Disk resonator gyroscope with whole-angle mode operation," *IEEE International Symposium on Inertial Sensors and Systems (ISISS), 2015,* Hapuna Beach, HI, 23-26 March 2015.

[7] V. Kaajakari, T. Mattila, A. Oja, H. Seppä "Nonlinear Limits for Single-Crystal Silicon Microresonators," *Journal of Microelectromechanical Systems* , vol.13, no.5, pp.715-724, Oct. 2004.

[8] I. Izyumin, M. H. Kline, Y.-C. Yeh, B. Eminoglu, C. H. Ahn, V. Hong, Y. Yang, E. J. Ng, T. W. Kenny, B. E. Boser "A 7ppm, 6°/hr frequency-output MEMS gyroscope" *28th IEEE MEMS Conference,* pp.33-36, 18-22 Jan. 2015.

[9] M. Agarwal, S. A. Chandorkar, R. N. Candler, B. Kim, M. A. Hopcroft, R. Melamud, C. M. Jha, T. W. Kenny, B. Murmann "Optimal drive condition for nonlinearity reduction in electrostatic microresonators" *Applied Physics Letters*, 89, 214105 (2006).

[10] S. Nitzan, T.-H. Su, C. H. Ahn, E. Ng, V. Hong, Y. Yang, T. Kenny, D. A. Horsley, "Impact of gyroscope operation above the critical bifurcation threshold on scale factor and bias instability," *27th IEEE MEMS Conference*, Jan. 2014, pp. 749–752.

CONTACT

*Parsa Taheri-Tehrani, tel: +1-530-341-3080; ptaheri@ucdavis.edu